A CONCEPTUAL DFT STUDY OF THE GEOMETRIC, OPTICAL PROPERTIES AND MOLECULAR DESCRIPTORS OF A VARIED ARRAY OF UREIDOPEPTIDOMIMETICS (UPM)

Y. Pavani[1] , S. Aravind[2] , M. Yanadirao[3] , K. V. Padmavathi[4] and M. Subba Rao[5]

[1]Assistant Professor, Department of Freshman Enigneering , PVP Siddhartha Institute of Technology (Affiliated to Jawaharlal Nehru Technological University Kakinada) Andhra Pradesh, India.

[2]Assistant Professor, Department Chemistry, University College of Sciences, Osmania University, Hyderabad, Telangana, India.

[3]Lecturer, Department of Chemistry, SKBR Govt. Degree College, Macherla, (Affiliated to Acharya Nagarjuna University) Andhra Pradesh, India.

[4]Lecturer, Department of Chemistry, TRR Govt. Degree College,(Affiliated to Acharya Nagarjuna University) Andhra Pradesh, India.

[5]Professor, Department of Chemistry, University College of Sciences, Acharya Nagarjuna University, Andhra Pradesh, India.

Abstract:

This study presents the geometry optimization of Ureidopeptidomimetics (UPM), along with analyses of frontier molecular orbitals, global reactivity descriptors, and absorption spectra. Utilizing density functional theory (DFT) with the B3LYP functional and 6-311++G(d,p) basis set, calculations were conducted in the gas phase and various solvents. The incorporation of electron acceptor groups at the ureido and carboxylate ends resulted in elongated C-O and C-N bond lengths in UPM due to their electron-accepting nature. CF_3-UPM exhibited the highest stability, as evidenced by lower HOMO energy and ionization values, indicative of reduced reactivity. Further assessments involving parameters such as η, S, and μ provided insights into connection stability. Excitation analyses revealed prominent peaks associated with n-to-π* or π-to-π* transitions, with the nature of these transitions influenced by the substituent groups. Notably, SH and COCl substituent's primarily contributed to π-to-π* transitions, while the CF3 group supported both n-to-π* and π-to-π* transitions.

Keywords: Ureidopeptidomimetics, DFT methods, Geometric, Optical Properties and Molecular descriptors.

INTRODUCTION

Ureidopeptidomimetics represent a promising class of synthetic compounds that mimic the structure and function of natural peptides, offering significant potential in medicinal chemistry and drug design [1, 2]. These analogs incorporate ureido groups, which enhance binding affinity

and specificity towards biological targets due to their unique hydrogen-bonding capabilities and structural flexibility [3]. The development of ureidopeptidomimetics aims to overcome limitations associated with natural peptides, such as poor bioavailability, rapid degradation by proteases, and limited cell permeability. By modifying the peptide backbone and introducing ureido linkages, researchers create more stable and bioactive compounds that retain or improve the biological activity of the parent peptides [4, 5]. One key advantage of ureidopeptidomimetics is their versatility in targeting a wide range of biological systems, including enzymes, receptors, and protein-protein interactions. For example, they have been successfully employed in the design of enzyme inhibitors, such as those targeting serine proteases, where the ureido group enhances the interaction with the enzyme's active site. Additionally, ureidopeptidomimetics show potential in modulating protein-protein interactions, which are often challenging targets in drug discovery [6,7].

Ureidopeptidomimetics, which have their peptide bonds (−C(O)NH−) replaced by urea (−HNC(O)NH−), have been synthesized with a variety of substituents on either end of the peptide chain [8–10]. These molecules show potential for applications in drug delivery, sensors, and molecular devices [11, 12]. The ureido group substitution for natural peptide bonds is known to alter the peptide backbone structure, thereby enhancing their functionality as proteins or enzymes [13]. This is attributed to the ureido group's ability to increase the likelihood of helical folding through hydrogen bonding interactions within biological systems [14]. Nonetheless, a significant challenge with UPs is their high water affinity, which results from their capacity to act as both hydrogen bond donors and acceptors [15]. Specifically, the ureido group's strong hydrogen bonding tendency makes them prone to proteolysis in the aqueous environments of cellular proteins [16]. Consequently, there is ongoing research to identify alternative compounds that retain the beneficial properties of UPs while being resistant to proteolysis in cellular aqueous environments.

Several substitutes for UP bonds have been proposed, wherein the oxygen in the urea carbonyl group is replaced with less electronegative elements from the chalcogen group, like sulfur and selenium [17]. Peptides containing sulfur typically display intriguing physical, chemical, and biological activities due to their lower electronegativity compared to regular peptides [18, 19]. It's anticipated that UP derivatives would exhibit similar behavior [20–22]. An examination of

their electronic, absorption, and charge transfer properties could highlight their diverse applications in fields like photoswitches and photosensors. To this end, we conducted studies on the electronic structures in both ground and excited states, alongside their absorption properties. Moreover, we explored the substantial role of UPs in charge transduction by creating a hole at the donor and mobilizing the electron at the vertically ionized state, employing density functional theoretical (DFT) methods.

Over the past decade, there has been a significant increase in the use of computational methods for peptide and protein design, with new examples emerging almost weekly, if not daily. This growth is attributed to several factors, including rapid advancements in computer technology, the availability of both commercial and freeware software packages for molecular modeling, and easy access to various databases such as the Cambridge Structural Database (CSD), the Protein Data Bank (PDB), and Swiss-Prot/TrEMBL. Additionally, there is now broad consensus that computational approaches, alongside experimental methods, are critical components of the drug design pipeline. Computational chemistry and molecular modeling have been instrumental in the rational design and optimization of ureidopeptidomimetics, providing valuable insights into their conformational properties and interaction mechanisms with biological targets [23].

Density functional theory (DFT) [24], initially developed for solid-state physics problems, has become a valuable tool for molecular structure calculations [25]. This method incorporates electron correlation effects, whose full impact on conformational energetics is still being quantitatively evaluated. Traditionally, DFT calculations were performed using local density functionals (LDF). However, recent trends show a preference for gradient-corrected density nonlocal functionals (NLF) [26, 27], which are regarded as more accurate than LDF in predicting geometries and conformational energetics. NLDFT is not only computationally efficient but has also been shown in the literature to provide accuracy comparable to, and often better than, conventional post-Hartree–Fock methods.

EXPERIMENTAL

Computational Methods

All calculations were performed using the Gaussian 09 software package [28]. Ground state electronic structures of ADP molecules were optimized using Density Functional Theory (DFT),

while Time-Dependent Density Functional Theory (TD-DFT) was employed for optimizing the excited state structures. TD-DFT is recognized as an effective method for describing excited states. For all calculations, Becke's three-parameter hybrid exchange functional combined with the Lee-Yang-Parr correlation (B3LYP functional) and the B3LYP / 6-31++G(d,p) basis set were utilized [29, 30]. The Polarizable Continuum Model (PCM) was used to study the solvent effects on the molecules, as PCM is known to provide a reliable treatment for biological molecules [31]. The solvents used in this study included methanol (ε = 32.6), acetonitrile (ε = 37.5), DMSO (ε = 47), and water (ε = 78.5). Excited-state calculations were carried out using TDDFT, and geometry optimization at the first excited state was performed to understand the geometrical changes occurring in this state. Additionally, the CAM-B3LYP functional was used, as it has been shown to provide accurate results for studying excited states without the correlation between error and spatial orbital overlap values (λ) for similar molecules [32].

RESULTS AND DISCUSSIONS

The models investigated in this study have been visually depicted in Figure 1 and are enumerated in Figure 2. The UPM models utilized for the computations were generated by substituting electron acceptors in both the ureido group side and the carboxylic side. These models are designated as A1-UPM, A2-UPM, A3-UPM, M1, UPM-A1, UPM-A2, and UPM-A3, with A1 representing -SH, A2 representing -COCl, and A3 representing -CF_3. Each model comprises both A-UPM and UPM-A components, as illustrated in Figures 1 and 2. The distinguishing factor among them is the acceptor groups between the ureido and carboxylate ends, thereby extending the peptide chain length. This setup enables the comparison of results regarding the influence and reproducibility concerning the distance between the donor and acceptor.

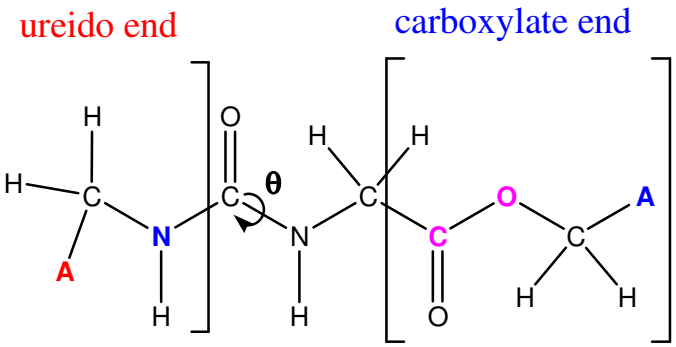

Model UPM ; ureido end :A-UPM model ; carboxylate end:UPM-A model
A1=-SH, A2= -COCl, A3=-CF_3

FIGURE 1 Schematic representation of different models studied in the work, (A1=-SH, A2= -COCl, A3=-CF_3) (**θ** represents the dihedral angle of the peptide bond)

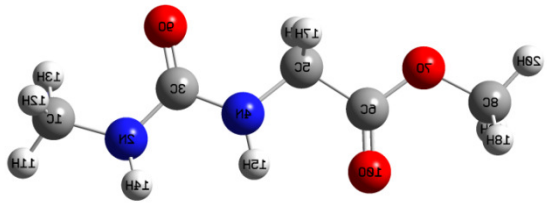

UPM

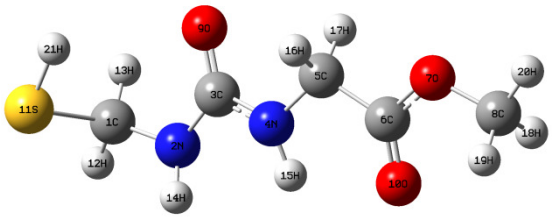

HS-UPM

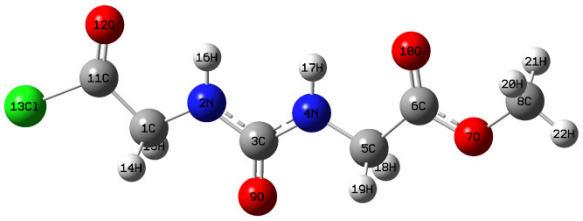

ClOC-UPM

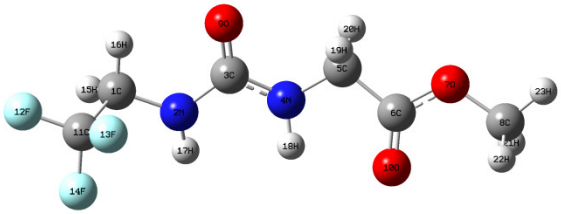

CF_3-UPM

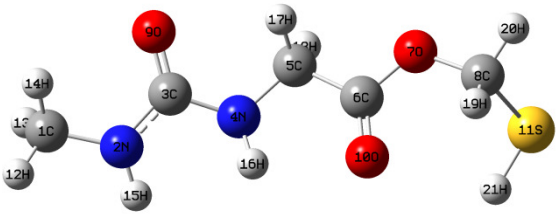

UPM-SH

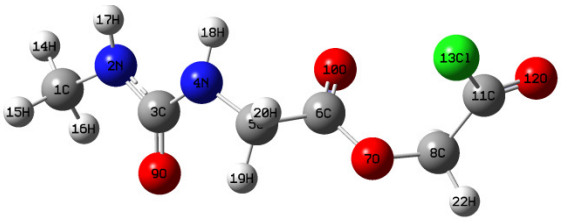

UPM-COCl

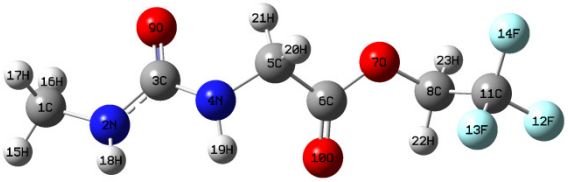

UPM-CF_3

Fig. 2: The Geometry optimized structures for A-UPM and UPM-R models in the gas phase. (A1=-SH, A2= CH_2Cl, A3= -COCl, A4=-CF_3)

Structural and electronic properties

In this study, utilizing the DFT/B3LYP method for the ground state and the TD-DFT/B3LYP method for the excited state, the optimized structures of all UPM models of molecules were obtained. Figure 2 presents the optimized geometrical structures, while Tables 1 and 2 contain a list of the parameters. All models are reported with their energetics analyzed and optimized in this work. The relaxation process indicates that, similar to natural peptides and unsubstituted UPMs, the conformers with all of their bonds oriented trans to one another possess the lowest energy. Analysis of the structural parameters reveals that, compared to unsubstituted UPM, the substitution of electron donor groups at the ureido and carboxylate ends shortens the C-O and C-N bond distances in UPM by 0.005 Å and 0.0003 Å, respectively (Tables 1 and 2). This phenomenon is attributed to the electron-donating nature of the substitution. Regardless of the models employed here, the groups substituted at the ureido end exhibit their capability to donate electrons, functioning as electron-rich groups.

The geometrical parameters of Ureidopeptidomimetics (UPM) were analyzed in different solvents (GAS, METH, ACET, DMSO, WATER) using Density Functional Theory (DFT). The parameters include bond lengths (rC–A, rC–N, rC=O, RO–C, RC=O) and bond angles (N–C–A). These parameters were evaluated to understand the influence of solvent environments on the molecular geometry and stability of various UPM derivatives. The study shows that the geometric parameters of UPMs are generally sensitive to the solvent environment, with polar solvents like water and DMSO inducing notable changes in bond lengths and angles compared to gas. The ureido and carboxylate ends of the molecules respond differently to salvation, with the carbonyl bonds showing the most significant changes. This is likely due to the polar nature of these bonds, which interact more strongly with polar solvents through dipole interactions and hydrogen bonding.

Implications for Molecular Stability and Reactivity

The observed changes in bond lengths and angles due to solvent effects imply that the stability and reactivity of UPMs can be significantly influenced by the solvent environment. Longer bond lengths in polar solvents suggest increased flexibility and potential for interaction with other molecules or ions in solution. This information is crucial for designing UPMs for specific applications, such as drug delivery or as catalysts in chemical reactions, where the solvent environment can be optimized to enhance desired properties.

Table 1. Structural parameters (bond length (A) and bond angles (˚)) of R-UPM model studied at the neutral state using DFT/B3LYP/6-311++G(d,p) basis set.

Solvent	**ureido end**				**carboxylate end**	
	r_{C-A}	r_{C-N}	$r_{C=O}$	**N–C–A**	R_{O-C}	$R_{C=O}$
	UPM					
GAS	-----	1.45663	1.23089	-----	1.21662	1.44352
METH	-----	1.45716	1.24354	-----	1.21942	1.44899
ACET	-----	1.45716	1.24362	-----	1.21943	1.44901
DMSO	-----	1.45714	1.24380	-----	1.21946	1.44906
WATER	-----	1.45711	1.24404	-----	1.21948	1.44912
HS-UPM						
GAS	1.8585	1.3905	1.2309	115.9679	1.341	1.2164
METH	1.8673	1.3827	1.2406	115.8933	1.3352	1.2193
ACET	1.8674	1.3826	1.2407	115.8915	1.3351	1.2193
DMSO	1.8673	1.3827	1.2406	115.8941	1.3352	1.2193
WATER	1.8675	1.3824	1.2409	115.8889	1.335	1.2194
ClOC-UPM						
GAS	1.506	1.3717	1.2428	110.1291	1.3352	1.2194
METH	1.508	1.3782	1.233	109.9158	1.341	1.2163
ACET	1.506	1.3719	1.2425	110.1238	1.3353	1.2193
DMSO	1.506	1.3718	1.2427	110.1261	1.3353	1.2193
WATER	1.506	1.372	1.2425	110.1228	1.3353	1.2193
CF_3-UPM						
GAS	1.5224	1.3869	1.2296	112.1575	1.3405	1.2165
METH	1.5234	1.3812	1.24	112.516	1.3351	1.2193
ACET	1.5234	1.3812	1.2401	112.5071	1.3351	1.2193
DMSO	1.5234	1.3814	1.2399	112.4996	1.3351	1.2193
WATER	1.5234	1.381	1.2403	112.5016	1.335	1.2194

Table 2. Structural parameters (bond length (A) and bond angles (˚)) of UPM-A model studied at the neutral state using DFT/B3LYP/6-311++G(d,p) basis set.

Solvent	**ureido end**		**carboxylate end**			
	r_{C-N}	$r_{C=O}$	R_{O-C}	$R_{C=O}$	r_{C-A}	r_{O-C-A}
	UPM					
GAS	1.45663	1.23089	1.21662	1.44352	-----	-----
METH	1.45716	1.24354	1.21942	1.44899	-----	-----
ACET	1.45716	1.24362	1.21943	1.44901	-----	-----
DMSO	1.45714	1.24380	1.21946	1.44906	-----	-----
WATER	1.45711	1.24404	1.21948	1.44912	-----	-----
UPM- SH						
GAS	1.3789	1.2304	1.3474	1.2167	1.8225	114.3905
METH	1.3687	1.2432	1.3448	1.2175	1.8235	113.907
ACET	1.3685	1.2435	1.3448	1.2175	1.8235	113.8992
DMSO	1.3688	1.2432	1.3448	1.2175	1.8235	113.909
WATER	1.3683	1.2437	1.3448	1.2174	1.8236	113.8926
UPM-COCl						
GAS	1.3728	1.2289	1.3623	1.2097	1.5273	115.8502
METH	1.3641	1.2411	1.3584	1.2121	1.5233	115.3392
ACET	1.3641	1.2413	1.3583	1.2122	1.5232	115.3329
DMSO	1.3642	1.241	1.3584	1.2121	1.5233	115.3417
WATER	1.364	1.2415	1.3582	1.2122	1.5232	115.3243
UPM-CF_3						
GAS	1.3741	1.2293	1.3616	1.2102	1.5214	109.358
METH	1.3644	1.2411	1.3611	1.2105	1.5204	111.1507
ACET	1.3644	1.2413	1.3611	1.2105	1.5204	111.1532
DMSO	1.3644	1.2411	1.3612	1.2104	1.5204	111.1501
WATER	1.3643	1.2416	1.361	1.2106	1.5204	111.1551

Frontier molecular orbital's (FMOs)

Using the DFT method with B3LYP functional and 6-311++G (d,p) basis set, the Frontier Molecular Orbitals (FMOs) of the molecules under investigation were computed. Figures 3 and 4 display the molecular orbital structures in the gas phase for A-UPM and UPM-A models. The HOMO and LUMO energies, as well as the energy gap (ΔE) between them, were obtained for the gas phase and various solvents, as shown in Tables 3 and 4 and Figures 5 and 6.

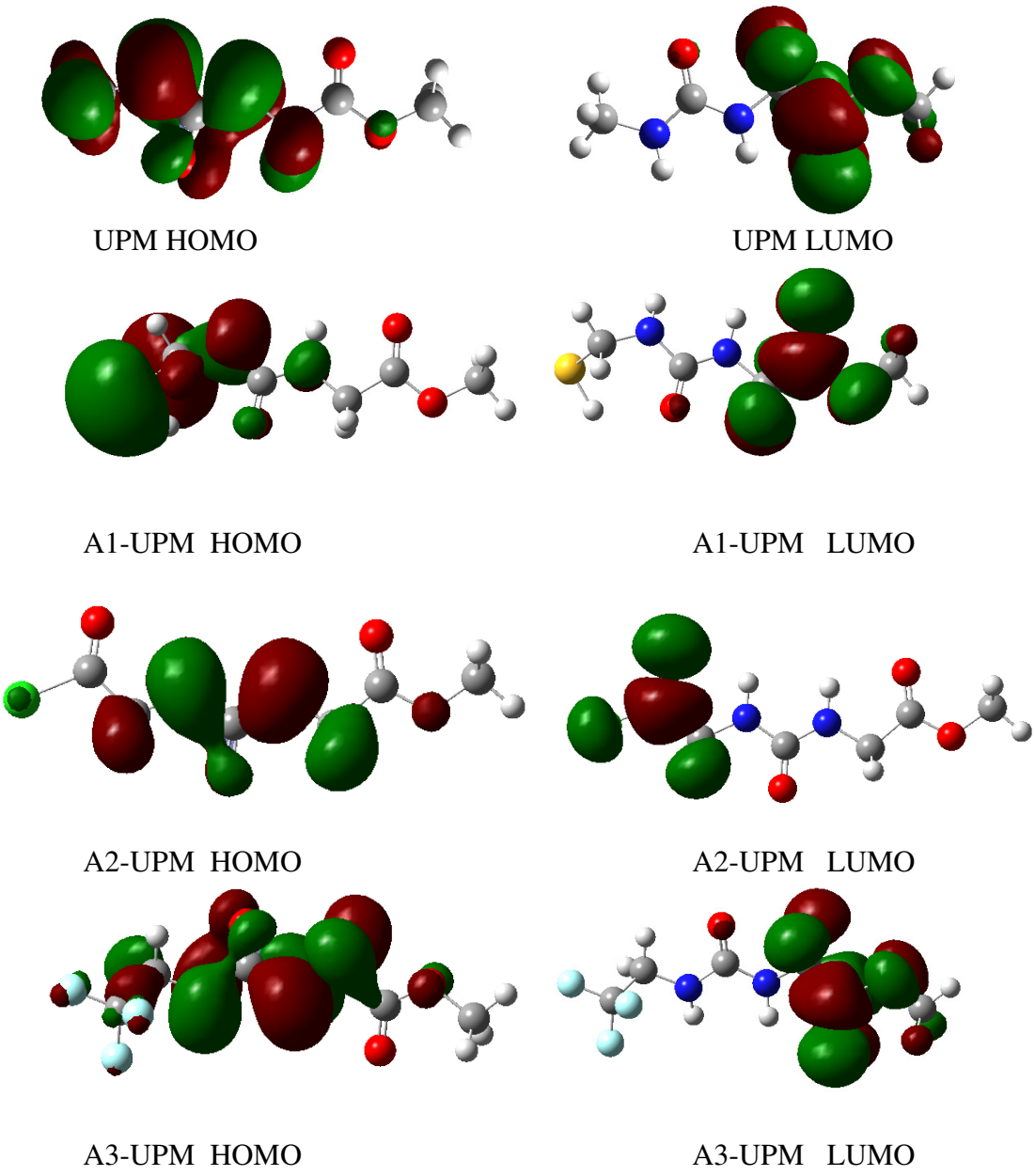

Fig. 3: HOMO and LUMO molecular orbital diagrams of the studied A-UPM model structures using B3LYP/ 6-311G++ (d,p) in the gas phase (A1=-SH, A2= CH_2Cl, A3= -COCl, A4=-CF_3).

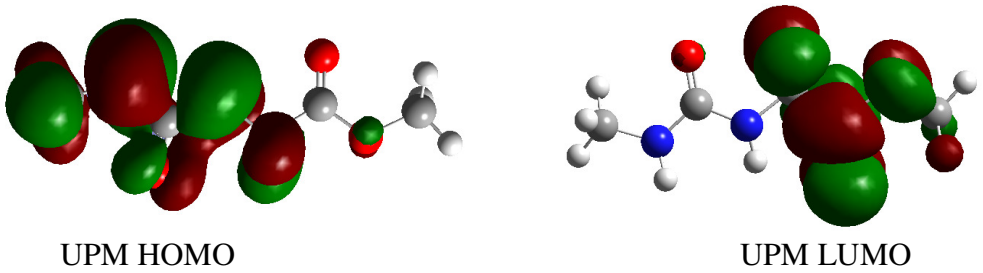

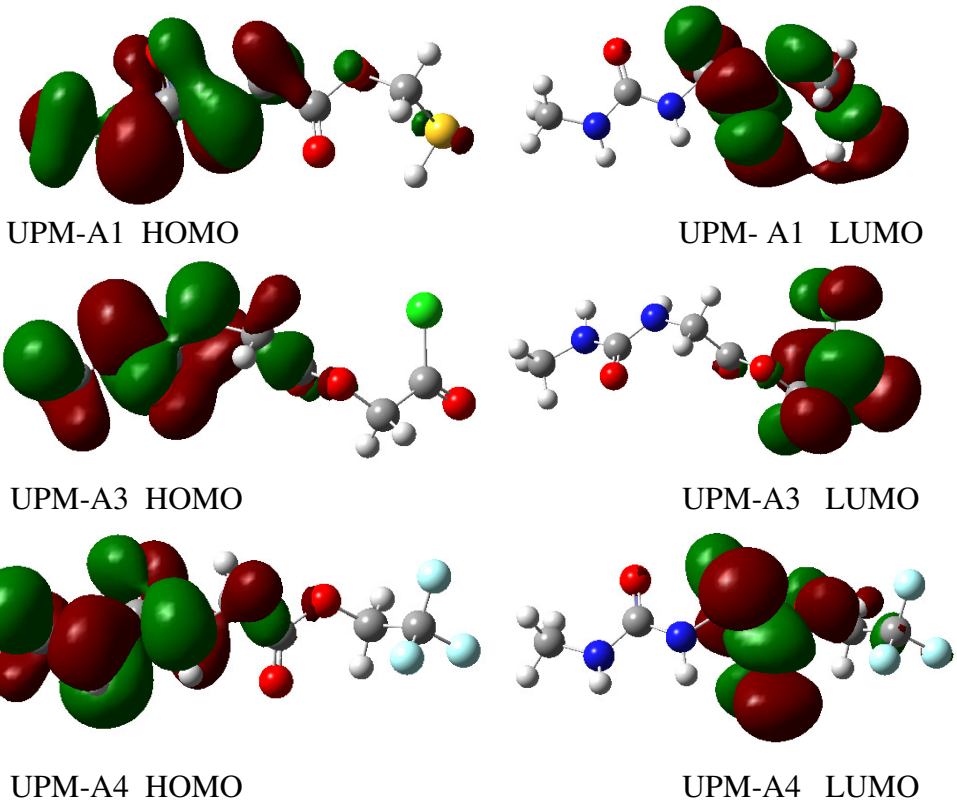

Fig. 3: HOMO and LUMO molecular orbital diagrams of the studied UPM-A model structures using B3LYP/ 6-311G++ (d,p) in the gas phase(A1=-SH, A2= CH_2Cl, A3= -COCl, A4=-CF_3).

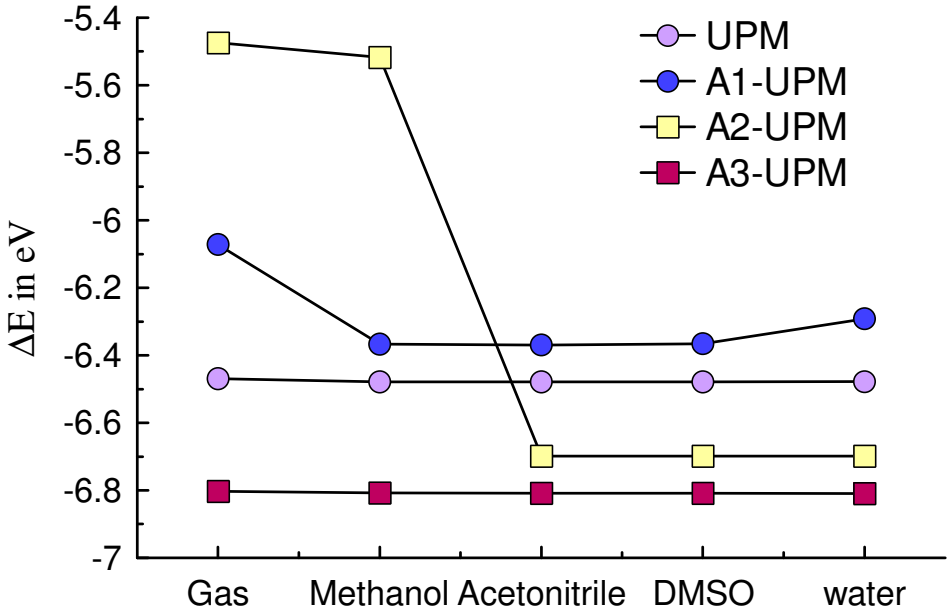

Fig. 5: The energy gap (ΔE) between HOMO and LUMO for studied model R-UPM in the gas and different solvents(A1=-SH, A2= CH_2Cl, A3= -COCl, A4=-CF_3).

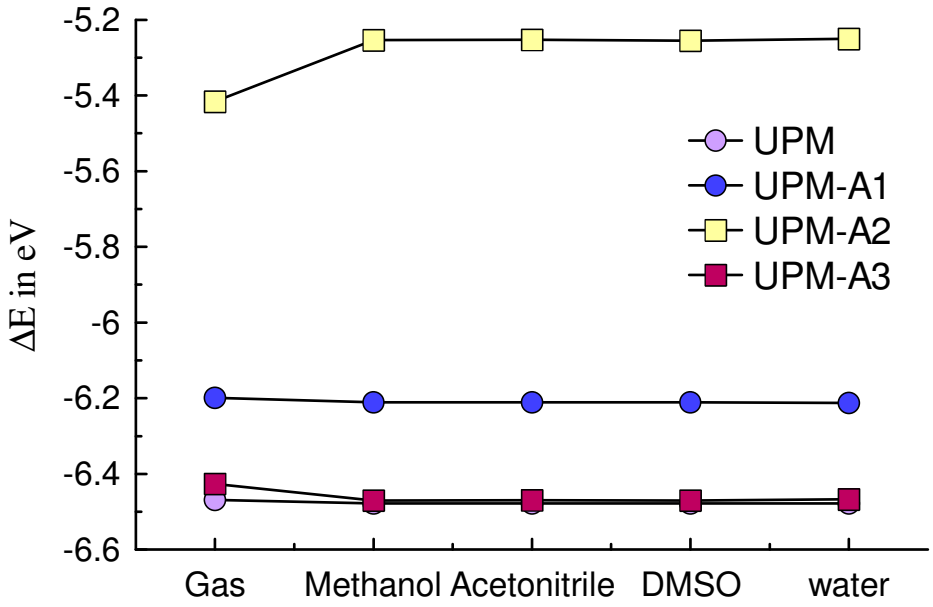

Fig .6: Fig. 5: The energy gap (ΔE) between HOMO and LUMO for studied model UPM-R in the gas and different solvents(A1=-SH, A2= CH_2Cl, A3= -COCl, A4=-CF_3).

The results section presents the findings from Table 3 and Figure 5, illustrating the energy gap (ΔE) variations for different Ureidopeptidomimetics (UPM) across diverse solvents: Gas, Methanol, Acetonitrile, DMSO, and Water. The UPMs analyzed include UPM, A1-UPM, A2-UPM, and A3-UPM. Across all solvents, the energy gap (ΔE) remains relatively stable. A slight increase is noted from Gas to DMSO, with values ranging between approximately 6.5 eV to 6.6 eV, the smallest observed in Gas and the largest in DMSO. A1-UPM maintains ΔE around 6.3 eV across all solvents, with minimal fluctuations. Methanol and Acetonitrile exhibit almost identical ΔE values, indicating similar solvation effects, while DMSO and Water show slightly higher ΔE compared to Gas. A2-UPM demonstrates an increasing trend in ΔE with solvent polarity, with ΔE ranging from 5.6 eV in Gas to around 6.4 eV in polar solvents like DMSO and Water. The highest ΔE is observed in Water, indicating substantial stabilization of the electronic structure. A3-UPM consistently displays the highest ΔE among all UPMs in every solvent, approximately 6.8 eV in Gas, slightly increasing in polar solvents like DMSO and Water, with ΔE remaining close to 6.9 eV across all solvents.

Moving on to the discussion, the focus is on the critical parameter of the energy gap (ΔE) and its influence on the electronic properties of molecules. The study analyzed the energy gaps of different UPM derivatives across various solvents to understand how solvent environments affect their electronic structures. Specifically, the discussion delves into the impact of solvent polarity on ΔE. Solvents range from non-polar (Gas) to highly polar (Water, DMSO), with polar solvents generally stabilizing the electronic structure of UPMs, leading to increased energy gaps. This trend is evident in A2-UPM and A3-UPM, where ΔE increases with solvent polarity. The behavior of each UPM derivative is scrutinized: UPM shows a moderate increase in ΔE with solvent polarity, A1-UPM exhibits minimal solvent effect, A2-UPM demonstrates a significant increase in ΔE from non-polar to polar solvents, and A3-UPM displays the highest ΔE values with minimal change across solvents, indicating strong intrinsic stability. The discussion also touches upon solvation effects, attributing the increase in ΔE in polar solvents to the stabilization of charged states of UPMs by solvent molecules, consequently increasing the energy gap.

The values of "DE" for UPM-A1 are quite similar across all solvents, with water having the highest value and gas having the lowest. This suggests that UPM-A1 has a relatively consistent interaction or behavior across these solvents, with water having the strongest interaction. The "ΔE" values for UPM-A2 vary more significantly across solvents compared to UPM-A1. Interestingly, the value is highest in water, which contrasts with UPM-A1, where gas had the lowest value. This suggests that UPM-A2 may have a different interaction profile or solubility behavior compared to UPM-A1.The "ΔE" values for UPM-A3 are quite similar across all solvents, with DMSO having the highest value and gas having the lowest, similar to UPM-A1. This suggests that UPM-A3 may have a consistent interaction profile or behavior across these solvents. The differences in "ΔE" values across solvents indicate differences in the solvation or interaction behavior of the compounds in different solvent environments.UPM-A2 shows more variability in "ΔE" values across solvents compared to UPM-A1 and UPM-A3, suggesting that its interaction with solvents may be more sensitive to solvent properties. The high "ΔE" values in water for UPM-A1 and UPM-A3 suggest strong interactions with water molecules, indicating potential hydrophilic characteristics.

Global chemical reactivity descriptors

The global chemical reactivity descriptors of the molecule, including the ionization potential, electron affinity, electronegativity, global softness, global hardness, chemical potential, and electrophilicity index, were determined using the FMO energies (E_{HOMO}, E_{LUMO}) [33, 34]. Electronegativity and hardness are two significant molecular properties that aid in interpreting and understanding the stability and reactivity of molecular systems [35].

Molecular descriptors obtained through quantum mechanical techniques have been extensively utilized in QSAR studies [36]. They calculate molecular volumes that describe shape, binding effects, and molecular reactivity. Among the most well-known quantum chemical descriptors are the HOMO and LUMO energies, as they represent the reactive species controlling numerous chemical reactions [37]. The HOMO energy quantifies the molecular sensitivity to electrophilic attacks and is directly linked to the ionization potential. Conversely, the LUMO energy indicates the molecule's susceptibility to nucleophilic attack and is directly associated with the electron affinity. Both the HOMO and LUMO energies govern radical reactions. Additionally, hard and soft nucleophiles, electrophiles, and molecule stability, as well as the active durability of HOMO and LUMO, can be succinctly defined.

The global reactivity descriptors, such as energy gap (Eg), ionizing potential (IP), affinity of electrons (EA), electron-negativity (χ), hardness (n), hardness (S), chemical potentials (μ), electrophilicity index (χ), charge-transfer (ΔNmax), nucleofugality (ΔEn), and electrofugality in gas phased form, are therefore determined using HOMO-LUMO energies.

$$\chi = -\frac{(E_{HOMO} + E_{LUMO})}{2} = \frac{I + A}{2} \quad \text{and} \quad \mu = \frac{(E_{HOMO} + E_{LUMO})}{2} \tag{2}$$

$$\eta = \frac{E_{LUMO} - E_{HOMO}}{2} \tag{3}$$

$$s = \frac{1}{2\eta} \tag{4}$$

$$\omega = \frac{\mu^2}{2\eta} \tag{5}$$

Two new reactivity indices, nucleofugality (ΔEn) and electrofugality (ΔEe) were proposed by Ayers and colleagues [38] to measure the ability of nucleophiles and electrophiles to leave the community. These indices are explained as follows.

$$\Delta E_n = -A + \omega = \frac{(\mu + \eta)^2}{2\eta} \tag{6}$$

$$\Delta E_e = I + \omega = \frac{(\mu - \eta)^2}{2\eta} \tag{7}$$

Table 3&4 displays the chemical and global descriptors for the following: ionization potential (IP), durability (S), softness (μ), charge transfer (ΔNmax), electrofugality, electronegative affinity (EA), electronegativity (χ), durability (S), softness (μ), and electrophilicity index (A).

In the models under study, the best electron donor is SH-UPM, which also exhibits the lowest ionization potential value (IP = 6.6279 eV) and the lowest HOMO energy (EHOMO = 0.5565 eV) (Tables 3 and 4). Based on the energy gap (ΔE) parameters, the compounds display varying levels of reactivity, with the compound OH-UPM being the most stable among them. The reactivity order is SH-UPM > COCl-UPM > CF3-UPM and UPM-COCl > UPM-SH > UPM-CF3.It's important to note that while these descriptors provide a simplified picture of a molecule's reactivity, they contain valuable information. Reactivity is a complex attribute influenced by various factors. For a comprehensive evaluation, it may be necessary to consider multiple descriptors and experimental data.

The best electron acceptor in the models under study is UPM-COCl, which has a higher electronegativity value. Higher electronegativity values indicate an atom's tendency to attract electrons into a covalent bond. When a molecule with high electronegativity interacts with other ions or in polar environments, it can become more reactive. Additionally, because the UPM-COCl model has a higher chemical potential, there is a greater likelihood that the system will undergo a chemical change, suggesting increased reactivity.

The data provides comprehensive insights into the electronic and energetic properties of the compounds in different solvent environments. Variations in these properties across solvents can indicate the influence of solvent polarity and interactions on the molecular structure and reactivity. Differences in ionization potential, electron affinity, and electronegativity across solvents reflect variations in the molecule's ability to donate or accept electrons. The

electrophilicity index and dipole moment can provide information about the molecule's reactivity and polarity, respectively. Understanding these properties is crucial for predicting chemical behavior, such as reactivity, solubility, and intermolecular interactions, in different solvent environments. Overall, the provided data offers valuable insights into the electronic and energetic characteristics of the compounds studied and their dependence on solvent properties. The observed variations in HOMO and LUMO energies across different solvents indicate that the electronic structure of the compounds is influenced by the solvent environment. Solvent polarity can affect the distribution of electron density within the molecule, leading to changes in energy levels.

Solvent polarity plays a significant role in determining the ionization potential, electron affinity, and electronegativity of the compounds. Polar solvents such as methanol and water can stabilize charged species more effectively than nonpolar solvents like gas, leading to differences in ionization potential and electron affinity. The calculated chemical hardness and softness provide insights into the reactivity of the compounds. Higher chemical hardness implies greater stability, while lower hardness suggests higher reactivity. The softness values reflect the polarizability of the molecules, which can influence their susceptibility to undergo chemical reactions. The electrophilicity index indicates the electrophilic nature of the compounds, reflecting their ability to accept electrons and undergo nucleophilic attack. Variations in electrophilicity across solvents can provide clues about solvent-dependent reactivity trends, with more polar solvents potentially enhancing electrophilic reactivity.

Table 3: Calculated Global chemical reactivity descriptors of the studied molecules in the gas and different solvents.

HOMO	LUMO	I	A	x	n	u	s	w	DN	DEn	DEe	DE	
UPM													
-6.8646	-0.3957	6.8646	0.3957	3.6302	3.2345	-3.6302	0.3092	2.0371	1.1223	1.6414	8.9017	-6.4689	**Gas**
-6.9027	-0.4242	6.9027	0.4242	3.6635	3.2393	-3.6635	0.3087	2.0716	1.1310	1.6474	8.9743	-6.4785	**Methanol**
-6.9027	-0.4245	6.9027	0.4245	3.6636	3.2391	-3.6636	0.3087	2.0719	1.1311	1.6474	8.9746	-6.4782	***Acetonitrile***
-6.9030	-0.4245	6.9030	0.4245	3.6638	3.2393	-3.6638	0.3087	2.0719	1.1310	1.6474	8.9749	-6.4785	**DMSO**
-6.9027	-0.4248	6.9027	0.4248	3.6638	3.2390	-3.6638	0.3087	2.0721	1.1312	1.6473	8.9748	-6.4779	**water**
A1- UPM													
-6.6279	-0.5565	6.6279	0.5565	3.5922	3.0357	-3.5922	0.3294	2.1253	1.1833	1.5689	8.7532	-6.0714	**Gas**
-6.8271	-0.4607	6.8271	0.4607	3.6439	3.1832	-3.6439	0.3142	2.0856	1.1447	1.6249	8.9127	-6.3664	***Acetonitrile***
-6.8292	-0.4599	6.8292	0.4599	3.6446	3.1847	-3.6446	0.3140	2.0854	1.1444	1.6255	8.9147	-6.3694	**DMSO**
-6.8263	-0.4610	6.8263	0.4610	3.6436	3.1826	-3.6436	0.3142	2.0857	1.1448	1.6247	8.9119	-6.3653	**Methanol**
-6.8320	-0.5404	6.8320	0.5404	3.6862	3.1458	-3.6862	0.3179	2.1597	1.1718	1.6193	8.9917	-6.2915	**water**
A2- UPM													
-7.1571	-1.6830	7.1571	1.6830	4.4201	2.7371	-4.4201	0.3654	3.5690	1.6149	1.8860	10.7261	-5.4741	Gas
-7.2347	-1.7176	7.2347	1.7176	4.4761	2.7586	-4.4761	0.3625	3.6316	1.6226	1.9140	10.8663	-5.5171	Methanol
-7.1588	-0.4599	7.1588	0.4599	3.8093	3.3495	-3.8093	0.2986	2.1662	1.1373	1.7063	9.3249	-6.6989	***Acetonitrile***
-7.1580	-0.4593	7.1580	0.4593	3.8086	3.3493	-3.8086	0.2986	2.1655	1.1371	1.7062	9.3234	-6.6986	DMSO
-7.1590	-0.4601	7.1590	0.4601	3.8096	3.3495	-3.8096	0.2986	2.1665	1.1374	1.7063	9.3255	-6.6989	water
A3- UPM													
-7.3884	-0.5859	7.3884	0.5859	3.9872	3.4013	-3.9872	0.2940	2.3370	1.1722	1.7511	9.7254	-6.8026	Gas
-7.2690	-0.4615	7.2690	0.4615	3.8652	3.4037	-3.8652	0.2938	2.1947	1.1356	1.7332	9.4636	-6.8075	Methanol
-7.2687	-0.4607	7.2687	0.4607	3.8647	3.4040	-3.8647	0.2938	2.1939	1.1353	1.7332	9.4626	-6.8080	***Acetonitrile***
-7.2703	-0.4620	7.2703	0.4620	3.8662	3.4041	-3.8662	0.2938	2.1955	1.1357	1.7334	9.4658	-6.8083	DMSO
-7.2682	-0.4593	7.2682	0.4593	3.8637	3.4044	-3.8637	0.2937	2.1925	1.1349	1.7332	9.4607	-6.8088	water

Table.4: Calculated Global chemical reactivity descriptors of the studied molecules in the gas and different solvents.

HOMO	LUMO	I	A	x	n	u	s	w	DN	DEn	DEe	DE	
UPM-A1													
-6.9678	-0.7690	6.9678	0.7690	3.8684	3.0994	-3.8684	0.3226	2.4141	1.2481	1.6451	9.3818	-6.1988	**Gas**
-6.9272	-0.7159	6.9272	0.7159	3.8216	3.1056	-3.8216	0.3220	2.3513	1.2305	1.6353	9.2785	-6.2113	***Acetonitrile***
-6.9267	-0.7151	6.9267	0.7151	3.8209	3.1058	-3.8209	0.3220	2.3503	1.2303	1.6352	9.2770	-6.2115	**DMSO**
-6.9272	-0.7162	6.9272	0.7162	3.8217	3.1055	-3.8217	0.3220	2.3515	1.2306	1.6353	9.2787	-6.2110	**Methanol**
-6.9267	-0.7140	6.9267	0.7140	3.8203	3.1063	-3.8203	0.3219	2.3492	1.2299	1.6352	9.2759	-6.2126	**water**
UPM- A2													
-7.2056	-1.7891	7.2056	1.7891	4.4974	2.7082	-4.4974	0.3692	3.7342	1.6606	1.9451	10.9398	-5.4164	Gas
-7.0766	-1.8223	7.0766	1.8223	4.4495	2.6271	-4.4495	0.3806	3.7680	1.6937	1.9456	10.8446	-5.2542	Methanol
-7.0763	-1.8234	7.0763	1.8234	4.4499	2.6264	-4.4499	0.3807	3.7696	1.6943	1.9462	10.8460	-5.2529	***Acetonitrile***
-7.0769	-1.8218	7.0769	1.8218	4.4493	2.6275	-4.4493	0.3806	3.7671	1.6934	1.9453	10.8440	-5.2551	DMSO
-7.0758	-1.8251	7.0758	1.8251	4.4504	2.6254	-4.4504	0.3809	3.7721	1.6952	1.9470	10.8479	-5.2507	water
UPM- A3													
-7.1691	-0.7426	7.1691	0.7426	3.9559	3.2133	-3.9559	0.3112	2.4350	1.2311	1.6924	9.6042	-6.4265	Gas
-7.0644	-0.5943	7.0644	0.5943	3.8293	3.2350	-3.8293	0.3091	2.2664	1.1837	1.6721	9.3308	-6.4701	Methanol
-7.0635	-0.5938	7.0635	0.5938	3.8286	3.2349	-3.8286	0.3091	2.2657	1.1835	1.6719	9.3292	-6.4698	***Acetonitrile***
-7.0644	-0.5940	7.0644	0.5940	3.8292	3.2352	-3.8292	0.3091	2.2661	1.1836	1.6721	9.3305	-6.4703	DMSO
-7.0633	-0.5962	7.0633	0.5962	3.8297	3.2335	-3.8297	0.3093	2.2679	1.1844	1.6717	9.3312	-6.4671	water

Differences in energy levels (ΔEn) between the HOMO and LUMO, as well as between the solute and solvent (ΔEe), highlight the interactions between the compounds and the surrounding solvent molecules. These interactions influence the stability and energetics of the solute-solvent system, affecting properties such as solubility and chemical reactivity. The dipole moment values provide insights into the polarity of the compounds and their interaction with polar solvent molecules. Higher dipole moments indicate greater polarity, which can lead to stronger dipole-dipole interactions between the solute and solvent molecules.

Excited states and absorption spectra

Using the TD/DFT method for the gas phase and the PCM-TD/DFT method for the solvent phase, the excited states of the molecules were calculated. Table 5 displays the values for the oscillator strength (f), excitation energy (Ex), maximum absorption wavelength (λmax), and significant MO assignments in both the gas and solvent phases for the R-UPM model. The maximum values of the studied molecules (A1–A3) range from 218.67 to 209.89 nm and 228.00 to 221.00 nm for A-UPM and UPM-A models, respectively. The first excited state in the Franck-Condon region corresponds to the change from the highest energy occupied molecular orbital to the lowest energy molecular orbital, based on results from calculations conducted in both the gas and solvent phases. The first excited state correlates to the transition from HOMO to LUMO, while the second excited state corresponds to the HOMO -> LUMO +1 transition, based on data from solvent phase calculations. Figures 7-10 illustrate how the absorption spectra of the investigated molecules differ in terms of spectral region pattern in the two environments. The dominance of the HOMO→LUMO transition has been revealed by comparing the results for the two environments.

The electronic structure of the peptide backbone undergoes significant alteration, along with its polarization, when UPMs are substituted with different acceptor units (SH, COCl, and CF_3). This alteration results in a shift in the negative charge polarization of the un-substituted UPM from the ureido group towards the end where the substituent is located. Excitation calculations reveal two sharp peaks corresponding to transitions from n to π* or π to π*, where π and n are localized at distinct energy levels depending on the substituent groups selected. The SH and CF_3 substituents in UPM predominantly contribute to π to π* transitions, whereas the COCl groups favor both π to π* and n to π* transitions. Excitation studies demonstrate that, except for the SH-

UPM model, all of the models exhibit strong peaks transitioning from one end to the other of the orbital's.

Table.5: Computed excitation wavelength (nm) and oscillator strength (f) of A1-UPM model computed using TD/DFT method in different solvents (A1= -SH, A2=-COCl, and A3=-CF_3)

UPM					
solvent	λ_{max} in eV	Wave length nm	f	orbital's	Contribution %
Gas	5.6705	218.67	0.0091	HOMO -> LUMO	81.05
Acetonitrile	5.6725	218.59	0.0102	HOMO -> LUMO	92.86
DMSO	5.6724	218.60	0.0102	HOMO -> LUMO	92.88
Methanol	5.6715	218.63	0.0105	HOMO -> LUMO	92.92
water	5.6726	218.59	0.0102	HOMO -> LUMO	93.05
					A1-UPM
Gas	5.3600	231.32	0.0107	HOMO -> LUMO+2	0.56536
Acetonitrile	5.4988	225.47	0.0063	HOMO-1 -> LUMO+2	0.13007
DMSO	5.4972	225.54	0.0065	HOMO-1 -> LUMO+2	-0.14835
Methanol	5.4990	225.47	0.0062	HOMO-1 -> LUMO+2	0.12913
water	5.5024	225.33	0.0062	HOMO-1 -> LUMO+2	0.13450
					A2-UPM
Gas	4.6254	240.56	0.0145	HOMO-1 -> LUMO+2	0.2578
Acetonitrile	4.7318	262.02	0.0162	HOMO-1 -> LUMO+2	0.26735
DMSO	4.6826	264.77	0.0209	HOMO-1 -> LUMO+2	0.19150
Methanol	4.6814	264.84	0.0214	HOMO-1 -> LUMO+2	0.19119
water	4.6829	264.76	0.0208	HOMO-1 -> LUMO+2	0.19169
					A3-UPM
Gas	5.9070	209.89	0.0082	HOMO-2 -> LUMO	-0.13942
Acetonitrile	5.9237	209.30	0.0124	HOMO-1 -> LUMO	-0.13194
DMSO	5.9237	209.30	0.0124	HOMO-1 -> LUMO	-0.13194
Methanol	5.9247	209.27	0.0120	HOMO-1 -> LUMO	-0.13136
water	5.9258	209.23	0.0121	HOMO-1 -> LUMO	-0.13139

Table.6: Computed excitation wavelength (nm) and oscillator strength (f) of UPM-A model computed using TD/DFT method in different solvents (A1= -SH, A2=-COCl, and A3=-CF_3)

UPM					
solvent	λ_{max} in eV	Wave length nm	f	orbital's	Contribution %
Gas	5.6705	218.67	0.0091	HOMO -> LUMO	81.05
Acetonitrile	5.6725	218.59	0.0102	HOMO -> LUMO	92.86
DMSO	5.6724	218.60	0.0102	HOMO -> LUMO	92.88
Methanol	5.6715	218.63	0.0105	HOMO -> LUMO	92.92
water	5.6726	218.59	0.0102	HOMO -> LUMO	93.05
UPM-A1					
Gas	5.4353	228.11	0.0184	HOMO-1 -> LUMO	0.33112
Acetonitrile	5.4411	227.87	0.0175	HOMO -2-> LUMO	0.16767
DMSO	5.4405	227.89	0.0178	HOMO-2 -> LUMO	0.16758
Methanol	5.4410	227.87	0.0174	HOMO-2 -> LUMO	0.16776
water	5.4424	227.81	0.0173	HOMO-2 -> LUMO	0.16648
UPM- A2					
Gas	4.9709	249.42	0.0017	HOMO-3 -> LUMO	0.28955
Acetonitrile	4.7970	258.46	0.0064	HOMO -1-> LUMO	0.69822
DMSO	4.7950	258.57	0.0066	HOMO-1 -> LUMO	0.69830
Methanol	4.7977	258.42	0.0063	HOMO-1 -> LUMO	0.69818
water	4.7926	258.70	0.0065	HOMO-1 -> LUMO	0.69849
UPM- A3					
Gas	5.6003	221.39	0.0039	HOMO-3 -> LUMO	-0.13433
Acetonitrile	5.5734	222.46	0.0008	HOMO-3 -> LUMO	-0.18147
DMSO	5.5716	222.53	0.0009	HOMO-3 -> LUMO	-0.18079
Methanol	5.5740	222.43	0.0008	HOMO-3 -> LUMO	-0.18174
water	5.5704	222.58	0.0008	HOMO -> LUMO	-0.17952

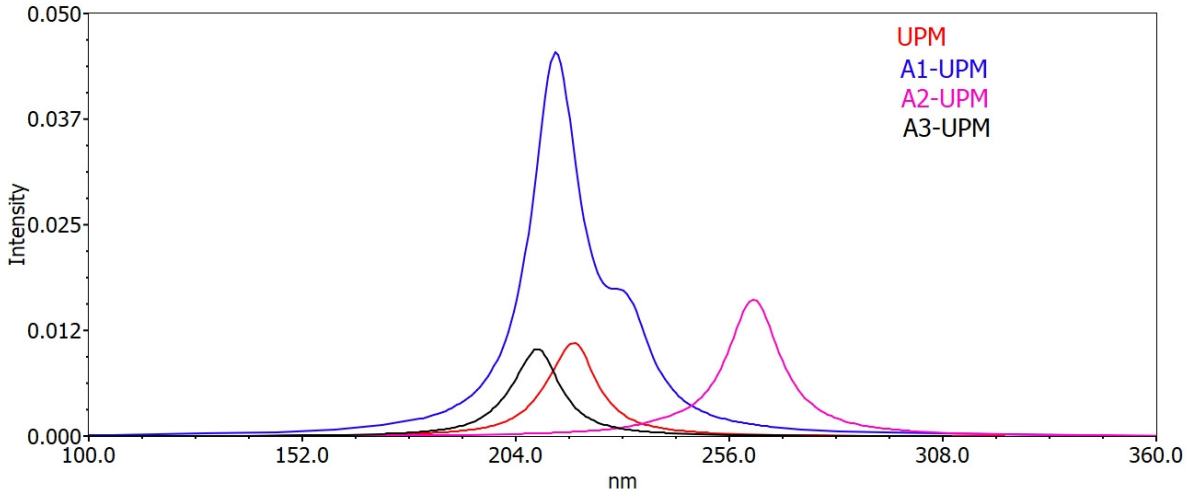

Fig.7: Simulated UV–visible optical absorption spectra of the studied molecules of model A-UPM (A1= -SH, A2=-COCl, and A3=-CF_3) with calculated data at the TD-DFT/B3LYP/6-311++ G (d,p) level in gas phase.

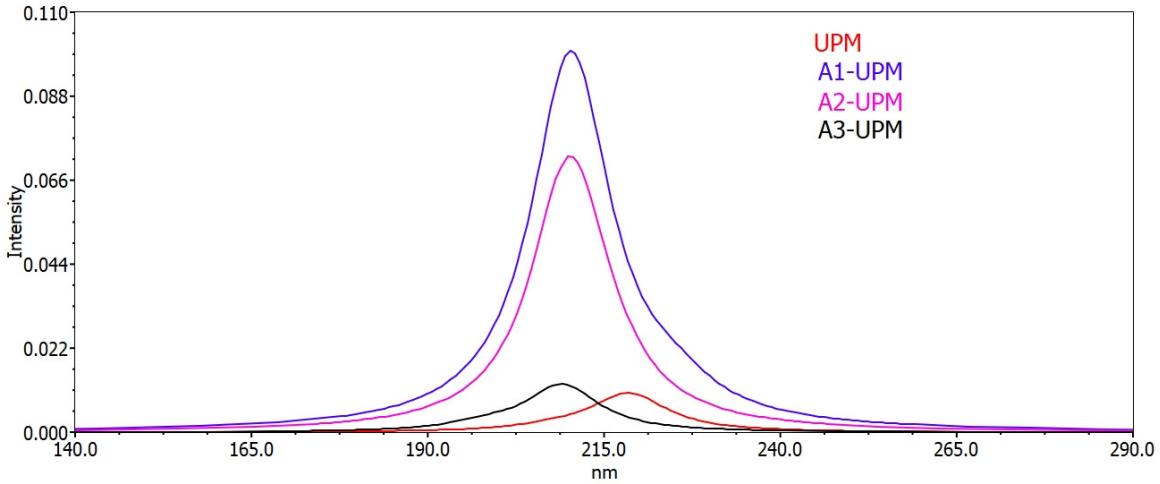

Fig.8: Simulated UV–visible optical absorption spectra of the studied molecules of model A-UPM (A1= -SH, A2=-COCl, and A3=-CF_3) with calculated data at the TD-DFT/B3LYP/6-311++ G (d,p) level in aqueous phase.

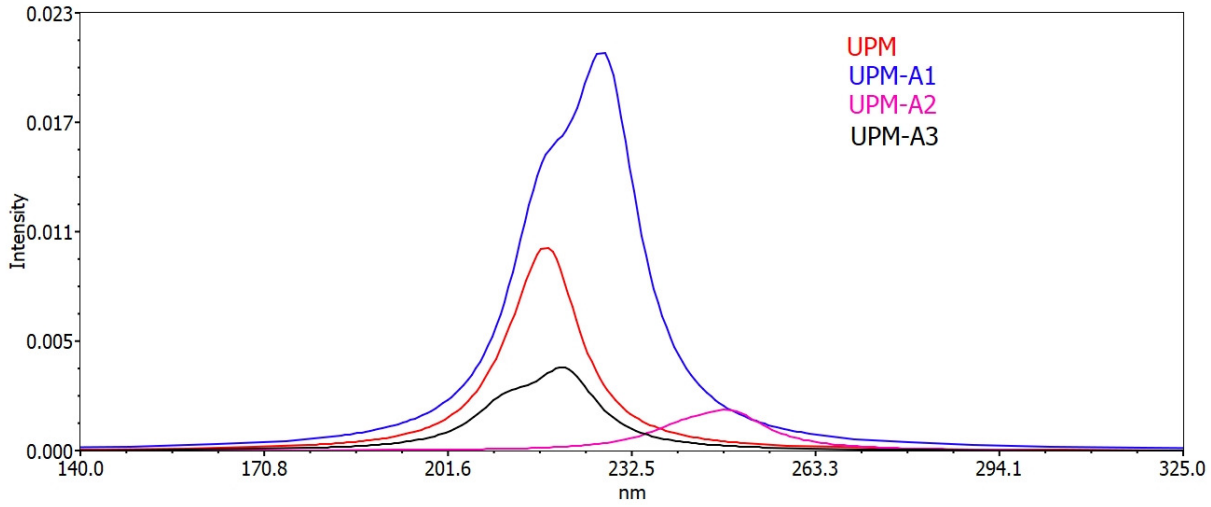

Fig.9: Simulated UV–visible optical absorption spectra of the studied molecules of model UPM-A (A1= -SH, A2=-COCl, and A3=-CF_3) with calculated data at the TD-DFT/B3LYP/6- 311++ G (d,p) level in gas phase.

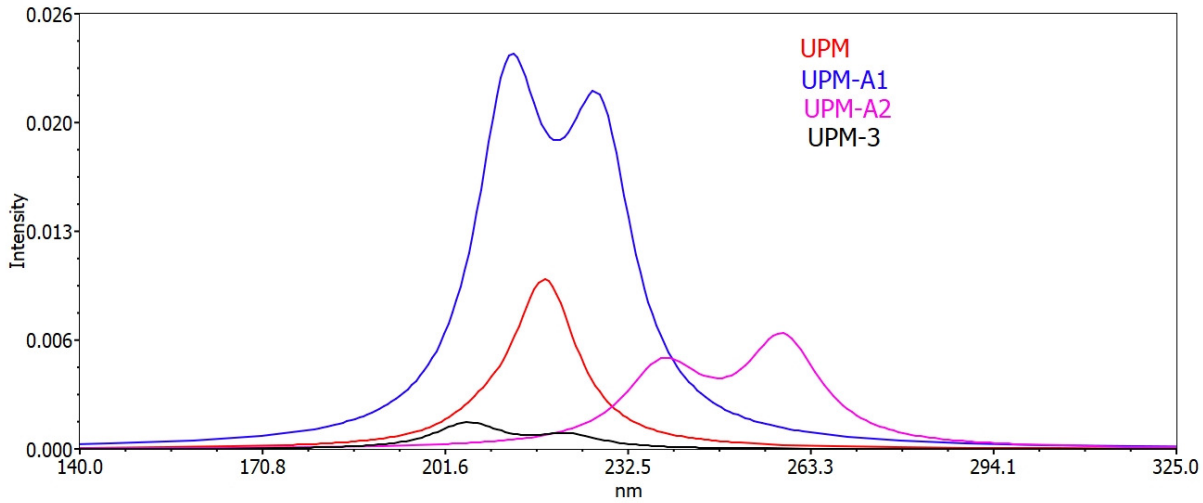

Fig.10: Simulated UV–visible optical absorption spectra of the studied molecules of model UPM-A (A1= -SH, A2=-COCl, and A3=-CF_3) with calculated data at the TD-DFT/B3LYP/6-311++ G (d,p) level in aqueous phase.

Conclusions

In this study, we conducted calculations using the Gaussian 09 package program, employing Density Functional Theory (DFT) for ground state optimization and Time-Dependent DFT (TDDFT) for excited state optimization. The results revealed that the introduction of electron

donor groups at the ureido and carboxylate ends of the UPM molecules led to shortened C-O and C-N bond distances, attributed to the electron-donating nature of the substitution. These structural changes indicate the potential for enhanced electron transfer capabilities in these molecules. Regarding molecular stability and reactivity, the observed changes in bond lengths and angles due to solvent effects suggest that the stability and reactivity of UPMs can be significantly influenced by the solvent environment. Polar solvents induce longer bond lengths, indicating increased flexibility and potential for interaction with other molecules or ions in solution. The analysis of the energy gap (ΔE) variations across different UPM derivatives and solvents revealed interesting trends. While ΔE remained relatively stable across all solvents for most UPMs, a slight increase was observed from gas to DMSO. A2-UPM and A3-UPM showed an increasing trend in ΔE with solvent polarity, with the highest ΔE observed in water.

References

1. S. Vagner, H. Qu, and J. Hruby, Curr. Opin. Chem. Biol, **12**, 292-296 (2008).
2. C. D. Schudok, et al. J. Med. Chem. **53**, (2010).
3. T. A. Knipe and J. M. Knipe, Drug Dev. Res. **71**, 150 (2010).
4. M. Fosgerau and T. Hoffmann, Drug Discov. Today **20**, 122 (2015).
5. P. E. Dawson and S. B. H. Kent, Annu. Rev. Biochem. **69**, 923 (2000).
6. J. J. Lenz and M. A. Schumacher, "Protein-protein interactions as drug targets," Curr. Opin. Chem. Biol. **5**, 371 (2001).
7. R. N. Warrington, Mol. Simul. **32**, 907 (2006).
8. G. Prabhu, N. Narendra, Basavaprabhu, V. Panduranga, V. V. Sureshbabu, RSC Adv. **5**, 48331(2015).
9. V. Semetey, C. Hemmerlin, C. Didierjean, A. P. Schaffner, A. G. Giner, A. Aubry, J. P. Briand, M. Marraud, G. Guichard, Org. Lett. **3**, 3843 (2001).
10. L. Fischer, V. Semetey, J. M. Lozano, A. P. Schaffner, J. P. Briand, C. Didierjean, G. Guichard, Eur. J. Org. Chem. 2007, 3944.
11. A. Boeijen, R. M. J. Liskamp, Eur. J. Org. Chem. 1999, 2127.

12. A. Devadoss, P. Sudhagar, C. Terashima, K. Nakata, A. Fujishima, J. Photochem. Photobiol. C: Photochem. Rev. **24**, 43 (2015).
13. J. Lapic, S. Djakovic, M. Cetina, K. Heinze, V. Rapic, Eur. J. Inorg. Chem. 106,2010.
14. A. M. Rincon, P. Prados, J. de Mendoza, J. Am. Chem. Soc. **123**, 3493 (2001).
15. M. D. Esrafili, J. Beheshtian, N. L. Hadipour, Int. J. Quantum Chem. **111**, 3184 (2011).
16. V. V. S. Babu, N. S. Sudarshan, S. A. Naik, Int. J. Pept. Res. Ther. **14**, 105 (2008).
17. Y. R. Nelli, S. Antunes, A. Salaun, E. Thinon, S. Massip, B. Kauffmann, C. Douat, G. Guichard, Chem.Eur. J.**21**, 2870 (2015).
18. E. E. Alberto, V. do Nascimento, A. L. Braga, J. Braz. Chem. Soc. **21**, 2032 (2010).
19. R. Pal, G. Nagendra, M. Samarasimhareddy, V. V. Sureshbabu, T. N. G. Row, Chem. Commun. **51**, 933 (2015).
20. S. Joy, V. V. Sureshbabu, G. Periyasamy, J. Phys. Chem. B **120**, 6469 (2016).
21. H. P. Hemantha, V. V. Sureshbabu, J. Pept. Sci. **16**, 644 (2010).
22. V. V. Sureshbabu, S. A. Naik, H. P. Hemantha, N. Narendra, U. Das, T. N. G. Row, J. Org. Chem. **74**, 5260 (2009).
23. S. H. Bertz, et al., J. Comput. Chem. **28**, 1183 (2007).
24. S. Liu and R. G. Parr, J. Comput. Chem, **20**, 2 (1999).
25. A. St. Amant, Rev. Comput. Chem, **7**, 217 (1999).
26. K. Raghavachari, J. Chem. Phys, **81**,1383 (1984).
27. C. Sosa, J. Andzelm, B. C. Elkin, E. Wimmer, K. D. Dobbs, J. A. Dixon J. Phys. Chem., **96**, 6630 (1992).
28. M. J. Frisch, G. W. Trucks, H. B. Schlegel, G. E. Scuseria, M. A. Robb, J. R. Cheeseman, D. J. Fox, Gaussian 09, Revision D.01, Gaussian, Wallingford, CT, USA (2009).
29. A. D. Becke, J. Chem. Phys. A **88**, (1988).
30. A. D. Becke, Phys. Rev. A **38**, 3098 (1988).
31. B. Mennucci, Wiley Interdiscip. Rev. Comput. Mol. Sci. **2**,386(2012).
32. M. J. G. Peach, P. Benfield, T. Helgaker, D. J. Tozer, J. Chem. Phys.**128**, (2008).
33. N. Boukabcha, A. Direm, M. Drissi, Y. Megrouss, N. Khelloul, N. Dege, M. Tuna, A. Chouaih, Inorg. Chem. Commun. **133**, 108884 (2021).
34. F. Mollaamin, M. Monajjemi, Mol. Simul. **49**, 365–376 (2023).

35. C. H. Suresh, G. S. Remya, P. K. Anjalikrishna, WIREs Comput. Mol. Sci. **12**, e1601 (2022).
36. M. Karelson, Molecular Descriptors in QSAR/QSPR; John Wiley & Sons, 2000.
37. Z. Zhou, Z. Pan, R. G. Parr, J. Am. Chem. Soc. **772,** 5720–5724 (1990).
38. G. Roos, S. Loverix, E. Brosens, et al., Chem. Biol. Chem. 7, 981 (2006).